Droplet Evaporation and Discharge Dynamics in Electrospray Ionization†

James N. Smith,*,‡ Richard C. Flagan,§ and J. L. Beauchamp||

Department of Environmental Engineering Science, Department of Chemical Engineering, Department of Chemistry, California Institute of Technology, Pasadena, California 91125

Received: March 5, 2002; In Final Form: June 28, 2002

We present measurements of the distributions of droplet size and charge along with, for selected droplets, the variation of droplet size and charge with time for electrosprays of methanol, acetonitrile, and water, as well as for methanol at different polarities and electrolyte concentrations. These measurements are performed using a new technique for measuring droplet size and charge that uses phase Doppler interferometry for obtaining droplet size and inferring droplet charge from comparison of measured and calculated droplet mobility in a constant electric field. For selected droplets, multiple measurements of the size and charge are performed by repeated reversal of the drift field. This "ping-pong" experiment tracks droplet size and charge for loss of up to 99.9% of the initial droplet volume. We observe that droplet instability, referred to as a discharge event, mainly occurs near or above the Rayleigh limit of charge, resulting in a charge loss of 15−20% for methanol and acetonitrile and 20−40% in the case of water. Each discharge event is accompanied by a small mass loss, and droplet size evolution is dominated by evaporation. Discharge dynamics for negatively charged droplets are similar to those observed for positively charged droplets. The addition of up to 10^{-4} M of NaCl to the solution does not significantly alter discharge dynamics. Measured size−charge correlations for droplets from electrosprays of methanol at low electrolyte concentrations ($<10^{-5}$ M), and to a lesser degree acetonitrile with similar electrolyte levels, fall into discrete groupings of size and charge that can be attributed to an initially monodisperse distribution of size and charge, followed by discharge events in which a nearly constant fractional charge loss occurs as a result of the Rayleigh instability.

Introduction

In recent years, the mechanism of electrospray ionization[1] has been the subject of extensive investigations using a variety of experimental methods. The physics of this phenomenon has intrigued researchers for over a century, beginning with Rayleigh's seminal paper in 1882[2] analyzing the instability resulting from evaporation of highly charged droplets. One reason for the current attention is the unique ability of electrospray ionization to create multiply charged molecular ions with very little dissociation, facilitating the study of high molecular weight biomolecules.[3] Although many details of the process are understood, important questions remain regarding the steps by which gas phase ions are eventually formed from the nascent highly charged droplets.[4] A complete understanding of the physical and chemical processes associated with electrospray ionization has implications both for the design of highly efficient ion sources and in correlating the observables in a mass spectrum with the nature and distribution of the analyte in solution and in the evolving charged droplets. Excellent reviews of the capabilities of electrospray ionization and the current understanding of the phenomenon can be found in two recent special journal issues.[5−13]

A typical electrospray setup is shown in Figure 1. A dilute solution of analyte in a volatile solvent is introduced through a small needle into a chamber in which dry nitrogen gas is passed at atmospheric pressure. An intense electrostatic field is formed at the tip of the needle by applying a few kilovolts potential difference between the needle and the chamber walls. At the tip of the needle, the strong electric field pulls liquid-phase ions toward the liquid−gas interface. The liquid surface at the tip of the needle forms a cusp, called a Taylor cone,[14] from the combined hydrodynamic and electrostatic forces, from which a fine spray of charged droplets is emitted. Evaporating charged droplets quickly reach a point at which they are no longer stable. This condition is known as "Rayleigh instability" after Lord Rayleigh's derivation, in 1882,[2] of the number of surface charges, Q_R, that exist on a droplet of radius, R_R, when

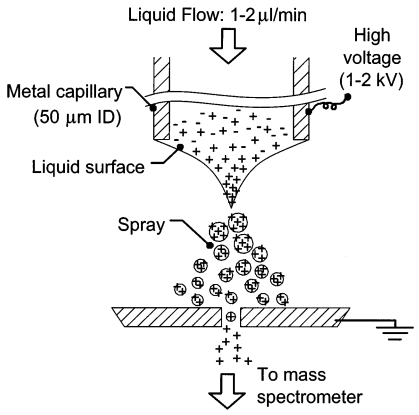

Figure 1. Schematic of the electrospray process. Typical values for these investigations are shown, where appropriate. The polarity of the applied field determines the polarity of the ions produced: the configuration for positive ions is depicted above.

† Part of the special issue "Jack Beauchamp Festschrift".

* To whom correspondence should be addressed. Present affiliation: National Center for Atmospheric Research. Phone: (303) 497-1468. Fax: (303) 497-1492. E-mail: jimsmith@ucar.edu.

‡ Department of Environmental Engineering Science.

§ Department of Chemical Engineering.

|| Department of Chemistry.

10.1021/jp025723e CCC: $22.00
Published on Web 08/24/2002

TABLE 1: Experimental Observations of Charged Droplet Breakup[a]

investigators	droplet diameter range studied (μm)	droplet solution	droplet charge at onset of instability (% Rayleigh limit)	mass loss for each disruption (%)	charge loss for each disruption (%)
Feng et al.[20]	ca. 84	methanol	not measured	not measured	81
Davis and Bridges[48]	4−20	water/surfactant	90	1−2	15−25
Gomez and Tang[23]	20−100	heptane	60−80	not measured	not measured
Taflin et al.[17]	4−20	low vapor pressure oils	75−85	2	10−15
Richardson et al.[54]	not reported	dioctylphthalate sulfuric acid	102 84	2.3 0.1	15 50
Schweitzer and Hanson[55]	15−40	*n*-octanol	96−104	5	23
Abbas and Latham[16]	30−200	Water, aniline, toluene	100	20−30	25

[a] All used electrodynamic balances with the exception of the Gomez and Tang study and are listed in reverse chronological order.

electrostatic repulsion is balanced by surface tension. This is given by eq 1, where ϵ_0 is the permittivity of free space and γ is the liquid surface tension:

$$Q_R = 8\pi(\epsilon_0 \gamma R_R^3)^{1/2} \quad (1)$$

One possible outcome of Rayleigh instability might involve the droplet breaking into two droplets of similar size and charge, an even fission process. Numerous experimental studies have shown, however, that the instability involves ejection of several similarly sized progeny droplets through the formation of what appears to be a Taylor cone on the parent droplet. The progeny droplets are much smaller than the parent. Interestingly, this was predicted by Rayleigh in 1882, who analyzed the instability and predicted that charge would be ejected from the droplet in a "fine jet". In the present paper, we will refer to this as a Rayleigh discharge event. Droplets produced in a discharge event will evaporate further, leading to additional instabilities. Eventually, gas-phase ions form from these droplets by two possible mechanisms. In the charged residue mechanism, a droplet becomes so small that it contains a single ion, thus further solvent evaporation leads to the formation of a gas phase ion. In the ion evaporation mechanism, solvated ions are emitted directly from charged droplets. These ions undergo further solvent evaporation to form gas-phase ions.

In the past century, numerous studies have attempted to follow the evolution of a charged droplet that has evaporated to Rayleigh's stability limit. Several key investigations are summarized in Table 1. Most studies of charged droplet instability resulting from evaporation have employed an electrodynamic balance (EDB)[15] to spatially confine a charged droplet for study, usually by sensitive optical techniques. The high volatility of solvents commonly used in electrospray ionization offers a challenge for investigators using an EDB to study the volatile solutions used in electrospray. As a result, many such studies have been performed mainly on slowly evaporating droplets such as water in a saturated bath gas[16] or low vapor pressure compounds such as hexadecane[17] and dodecanol.[18] The results of these investigations, included in Table 1, indicate general agreement for those studies involving low volatility solutions, with departures for sulfuric acid droplets[19] and more volatile methanol droplets.[20] The accepted mechanism of droplet discharge is primarily the result of the extrapolation of the EDB studies of the low-volatility compounds and can be summarized as follows. The limit of charge as set forth by Lord Rayleigh represents an upper limit in droplet stability, with most studies reporting disruption at charge levels of about 80% of the Rayleigh limit. Droplet charge is conserved during evaporation, and a charge loss of 10−25% accompanies each disruption event. Mass loss with each event is observed to be small, ranging from negligible to 5%.

The second method often applied to the study of electrosprays is phase Doppler interferometry (PDI).[21,22] PDI is an optical particle sizing technique that can perform in situ measurements of size and velocity of the electrosprayed droplets, providing more detailed information about the physical properties of actual electrosprays. Gomez and Tang[23] used this technique to study electrosprays of heptane. They obtained size distributions using PDI and calculated the average charge from a measurement of total droplet current using an electrode upon which the droplets impinged. Their results (see Table 1) set the threshold for disruption at 70−80% of the Rayleigh limit, attributing this low threshold for breakup to droplet distortion from aerodynamic stress. At large distances from the source, their size distributions feature a secondary peak at a diameter of 5 μm, which they conclude are the progeny droplets that result from droplet instability. Other phase Doppler studies of the electrospray process have focused on correlating the droplet size and velocity distributions with solution properties such as conductivity.[24] Naqui and co-workers[25] performed phase Doppler measurements on solutions of sulfuric acid and octanol and presented a plot of size versus velocity for one such spray. It shows a clear correlation of size with velocity, as well as discrete groupings resembling the results we have obtained for electrosprayed methanol droplets. Because their measurements were performed in the spatially inhomogeneous electric field surrounding the capillary, they could not make quantitative estimates of the droplet charge.

Other investigators have focused primarily on the properties of the progeny droplets that comprise the 1−5% mass fraction lost from the parent droplet following disruption. Photomicrographs of the process[23,26] suggest that this mass is carried off in an uneven fission process. In the EDB studies by Feng et al., methanol droplets were trapped in stable, oscillating orbits, and the change in intensity of the light scattered as the droplet passed through a laser beam was measured during each period of oscillation. Progeny droplets could be directly observed in the probe beam.[20] With methanol, they estimate that, on average, 13 droplets are produced in a single discharge event. Loscertales and Fernandez de la Mora[27] have cited investigations in their laboratory that show that the charge of the newly formed progeny droplets is 0.7 times the Rayleigh limit of charge for polar liquids such as those in the current study. Fernandez de la Mora and colleagues[11,27,28] have also carried out a series of experiments to detect and size progeny droplets and ions using the differential mobility analyzer (DMA).[29] Because the DMA is not generally suited for analyzing volatile droplets, they performed measurements on solid particle residues resulting from complete evaporation of the electrosprayed solution. Other investigators have made similar measurements,[30,31] which allowed for the calculation of the electric field at the droplet surface for which direct desorption of ions takes place, which ranges from 1 to 3 V/nm.

Investigations into the effect that solution properties have on electrospray behavior have focused primarily on electrical

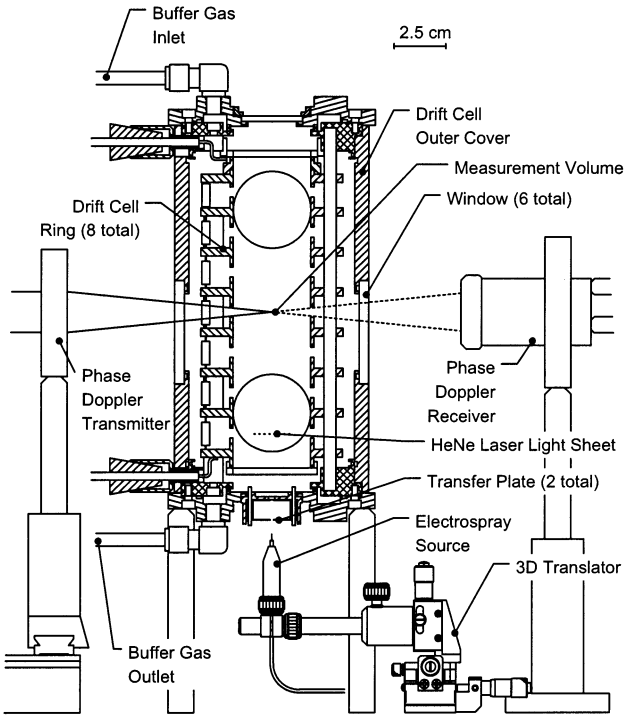

Figure 2. Experimental apparatus for studying droplet evaporation and discharge dynamics.

conductivity. Tang and Kebarle[32] have studied the effect that electrolyte concentration may have in ion formation in electrospray. They found a clear correlation between electrospray ion current and electrical conductivity of the solution over the range $10^{-6}-10^{-2}$ M. Other investigators have determined that the initial droplet diameter from an electrospray increases with decreasing bulk solution electrical conductivity.[33,34] Gañán-Calvo et al.[33] showed that the diameter varies as the inverse cube root of the electrical conductivity. Fernandez de la Mora[35] deduced that the droplet disruption process is quasistatic, meaning the lifetime of the Taylor cone is very large compared to the charge relaxation time. As a consequence, he calculated that the flow rate through the Taylor cone of a droplet undergoing disruption should be on the order of the quantity $\gamma\tau/\rho$, where γ is the bulk droplet surface tension, τ is the charge relaxation time, and ρ is the droplet density. Progeny droplet diameter should scale as the flow-independent characteristic length of the Taylor cone, $(\{\gamma\tau^2\}/\{\rho\})^{1/3}$. Both of these quantities are related to droplet electrolyte concentration through $\tau = \epsilon\epsilon_0/K$, where ϵ and ϵ_0 are the permittivities of the liquid and free space, respectively, and K is the electrical conductivity of the liquid.

The focus of the present work is on the mechanism and dynamics of droplet evaporation and discharge in electrospray ionization using the range of solvents commonly used in electrospray ionization, including for selected solvents, both positively and negatively charged droplets and a wide range of electrolyte concentrations. We have performed simultaneous, in situ measurements of the size and charge of droplets from an actual electrospray source, looking both at the correlation of size and charge in the spray as well as the time evolution of size and charge of selected individual electrosprayed droplets.

Experimental Section

Figure 2 shows a diagram of the apparatus used in this study. The electrospray source for these investigations employed a stainless steel capillary of 50 μm inside and 115 μm outside diameters biased in the range from $\pm$900 to $\pm$1200 V, the polarity of which determines the polarity of the droplets produced. A syringe pump delivers sample solution at flow rates of 0.2$-$1 μL/min. A three-dimensional translator positions the capillary at the entrance aperture to the drift cell. The tip of the electrospray needle is located approximately 2 mm from the first electrostatic transfer plate with a 1.5 mm aperture in the center. This plate is biased at 100 V. A second, identical plate is located 1 cm above the first and electrically grounded. These two transfer plates inject charged droplets from the spray source into the drift cell, while limiting the sampled droplets to those that are nominally coaxial with the drift cell. The spray can be sampled at various locations in the plume by adjusting the relative position of the capillary with respect to the first aperture. For these investigations, we sampled the spray directly on axis. We adjusted liquid flow rate and capillary voltage within the range listed above in order to create droplets in the diameter range of 5$-$40 μm. This creates droplets large enough to be monitored with optical techniques and long-lived enough to observe evaporation and discharge processes. Under these conditions, the electrospray operates in the "cone-jet" mode,[36] emitting a fine stream of droplets with a nearly monodisperse size distribution.

A uniform electric field within the drift cell, set to 51 V cm^{-1} in most of our experiments, is provided by eight resistively coupled, stainless steel rings. The interior of the cell is 13.8 mm in length and 3.8 mm in diameter. The rings have a "T"-shaped cross-section to shield the drift cell from field perturbations caused by the walls of the cell and to create uniform buffer gas flow conditions. We used an ion optics simulation program, SIMION,[37] to model the electric field within the cell. The simulation predicts that the electric field is constant over the length of the cell and the field is uniform to within 1% over the area enclosed by one-half the inner radius. Gaps of 5 mm between the rings provide optical access to the drift cell. Windows made from UV grade fused silica on the outer cover of the cell provide optical access to these gaps. A laminar countercurrent flow of nitrogen buffer gas is introduced into the drift cell at a rate of 0.3 L/min. Buffer gas temperature is monitored by inserting thermocouple probes at the top and bottom of the cell. The cell can be heated to a maximum temperature of 328 K with foil heating elements bonded to the outer cover.

The measurement volume of a phase Doppler interferometer (PDI), with a diameter of approximately 100 μm, is centered on the axis of the drift cell 10 cm above the source. For the conditions used in our experiments, this distance corresponds to a transit time for droplets emitted from the source to the measurement volume of approximately 200 ms. The PDI was built in-house for these investigations.[38] The optical system was not adjusted or moved following an extensive calibration procedure in the size range from 10 to 40 μm. The calibration consisted of using accurate velocity measurements from the PDI to determine the terminal velocities of a dispersion of falling water droplets and then calculating droplet aerodynamic diameter and comparing that to the measured diameter from the PDI. The well-established theory of phase Doppler interferometry allows the calibration to be extrapolated to the 1$-$10 μm range.[22] We also used SCATAP,[39] a phase Doppler simulation program based on Mie theory, to verify the linearity of the phase shift-diameter relationship in the diameter range 1$-$40 μm. From the calibration procedure, the measurement of diameter should be accurate to either $\pm$5% of the measured droplet diameter or $\pm$1 μm, whichever is larger. The velocity measurement is

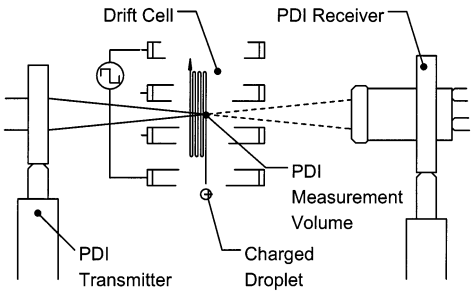

Figure 3. Droplet ping-pong measurement concept. Repeated reversal of the drift field permits multiple measurements of the size and charge of a single droplet

inherently more accurate, to ±0.2% based on literature values for similarly configured phase Doppler systems.[40] A LeCroy 9450A digital oscilloscope digitizes the phase Doppler signals. A software algorithm written in the LabVIEW programming language[41] processes the PDI signals using an FFT-based algorithm that determines the average frequency of the PDI signals and the phase shift between them.[42]

The experimental approach of this study is based on the fact that the charge on a droplet can be calculated by performing a simultaneous measurement of its size and velocity within a uniform electric field. This result emerges from a force balance calculation on an isolated droplet with charge, q, and is shown in eq 2.[43] In eq 2, α is either +1 or −1, depending on whether the droplet is traveling up or down, respectively; E is the constant electric field of strength; v_d is the droplet's steady-state drift velocity relative to the gas in the drift cell; q is the droplet charge; m_p and D_p are the mass and diameter of the droplet, respectively; ρ is the density of the surrounding gas; C_c is the slip correction factor; and C_D is the drag coefficient. The latter two parameters are found using established empirical relations[43] and depend only on droplet size and properties of the surrounding gas.

$$q = \frac{\pi C_D \rho D_p^2 v_d^2 - \alpha 8 C_c m_p g}{8 C_c E} \qquad (2)$$

The PDI is used to perform the measurements of droplet size and velocity. The uncertainties in droplet diameter and velocity noted above correspond to a measurement uncertainty for droplet charge of ±6%. Distributions of droplet size and charge of an electrospray, as well as a plot of droplet size versus charge (size-charge correlation), are obtained by introducing electrosprayed droplets into the drift cell and allowing them to pass into the measurement volume of the PDI.

We have also developed a new method for studying the time evolution of the size and charge of individual droplets from an electrospray source. The experimental methodology, which we refer to as a "ping-pong" experiment, is depicted in Figure 3. Charged droplets produced by an electrospray are introduced into the drift cell and allowed to pass through the measurement volume of the PDI. This results in a single size and charge measurement as described above. After a short delay, the electric field within the cell is reversed, and the droplet passes back through the measurement volume of the PDI for another size and charge measurement. The process is repeated until the droplet can no longer be detected by the PDI. This measurement provides the temporal evolution of the size and charge of selected droplets following their initial detection by the PDI.

For the ping-pong technique, an adjustable gain amplifier is installed between the receiver preamplifier and the signal digitizer to accommodate the decrease in scattered light intensity as the droplet evaporates. The digital oscilloscope is operated in sequential acquisition mode to minimize dead time between acquired signals. The trigger time for each phase Doppler signal in the ping-pong sequence is stored in the memory of the oscilloscope with the raw data from the PDI. These data are transferred to the computer via a GPIB interface once the digitizer acquires the full sequence of ping-pong measurements. The processed results, along with the raw signals, are stored to disk before the next sequence is acquired. The data acquisition system operates without user intervention, facilitating analysis of a large number of droplets.

We applied these measurement techniques to three solvents used commonly in electrospray ionization: filtered and deionized water, spectroscopic grade methanol, and spectroscopic grade acetonitrile. NaCl was added as noted whenever an electrolyte was required for studying the effect of electrolyte concentration. All experiments in this study were performed at atmospheric pressure and 293 K unless otherwise noted.

Results

Electrosprays of Methanol, Acetonitrile, and Water. We have examined the distribution of size and charge of droplets formed from a range of solvents commonly used in electrospray ionization, along with measurements of the evaporation and discharge dynamics of selected droplets. The solvents studied were spectroscopic grade methanol and acetonitrile as well as filtered, deionized water to which 10^{-4} M NaCl was added. We acquired size and charge distributions and size-charge correlations at a single spatial location on the spray axis. The electrospray source operated in positive-ion mode, resulting in positively charged droplets. Figures 4−6 show the results of these measurements. Figure 4 shows the data for water droplets. Because water is less volatile than the other solvents, the N_2 buffer gas in the drift cell was heated to 317 K to allow for observations of multiple discharge events. The size-charge correlation is presented in Figure 4c where it is compared to the Rayleigh limit. For droplets larger than 20 μm, the upper limit in charge lies below that corresponding to the Rayleigh limit. If droplet charge is conserved during evaporation and nascent droplets are approximately monodisperse in size, then the data for droplets larger than 20 μm describe droplets that are approaching the Rayleigh limit through solvent evaporation. As shown below, the rate of evaporation increases as droplet diameter decreases. Consequently, the smaller droplets are closer to the Rayleigh limit of charge. Droplets smaller than 20 μm in diameter carry a maximum charge that is 100% of the Rayleigh limit.

Data for acetonitrile droplets are shown in Figure 5. The diameter distribution, Figure 5a, suggests a high degree of monodispersity in the primary droplet distribution, with a steep slope on the large diameter side of the distribution and large tail on the small diameter side from droplet evaporation. Figure 5c shows the size-charge correlation for acetonitrile, with all of the droplets near the Rayleigh limit of charge. Unlike the case of water, all droplets sampled are within 15% of the Rayleigh stability limit and in fact may have undergone one or more discharge events prior to reaching the PDI sampling volume. Note that in this case some of the droplets survive with a charge slightly larger than the predicted Rayleigh limit.

Figure 6 shows the results of size and charge measurements for an electrospray of methanol. Structure is clearly evident in both the size and charge distributions. The size−charge correlations, Figure 6, parts c and d, suggest a mechanism that

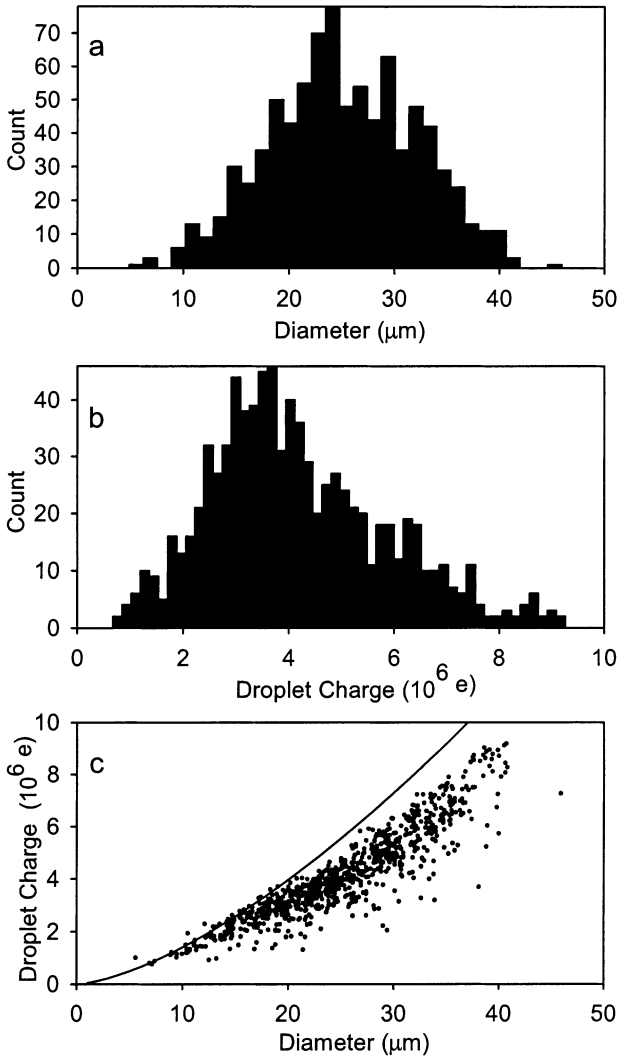

Figure 4. Plots of size and charge measurements of individual droplets in a positive-ion electrospray of 10^{-4} M NaCl in water. (a) Droplet diameter histogram; (b) droplet charge histogram; (c) diameter versus charge, plotted with a curve representing the Rayleigh stability limit.

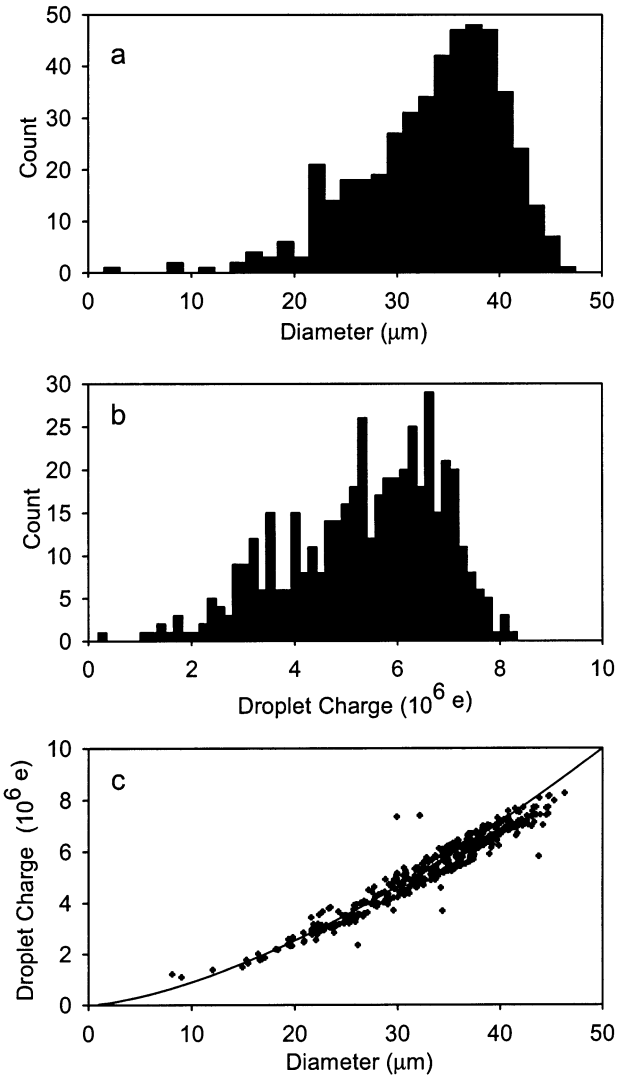

Figure 5. Plots of size and charge measurements of individual droplets in a positive-ion electrospray of pure acetonitrile. (a) Droplet diameter histogram; (b) droplet charge histogram; (c) diameter versus charge, plotted with a curve representing the Rayleigh stability limit.

originates with a nearly monodisperse stream of droplets created at the source, all with approximately the same diameter and charge. These droplets subsequently undergo evaporation−discharge cycles, and the small variation in nascent droplet size and charge result in similar fates for each droplet in the spray. The distinct groupings of droplets observed in the size charge correlation can be interpreted as three or more "generations" resulting from discharge processes. It is interesting to note that this fine structure was not observed in the electrospray of acetonitrile, even though as stated above the primary droplet distributions for both solutions appear to be monodispersed. One explanation for this is that the nascent droplets formed with the acetonitrile solution did not carry the same initial charge. As observed with acetonitrile, Figure 6d shows that methanol droplets survive with a charge larger than that predicted by the Rayleigh limit. It appears that discharge occurs when the charged exceeds the Rayleigh limit by up to 18%.

Although the data presented above provide a test of the Rayleigh criterion for droplet instability, little dynamic information can be inferred from single measurements on individual droplets. One possibility for obtaining further information would be to vary the drift voltage over a wide range. At higher drift voltages, for example, the distribution of charged droplets between the distinct charge groupings observed for methanol should shift to the right, because of the occurrence of fewer discharge events prior to sampling the droplets. A better approach, however, is the ping-pong technique, which can be employed to obtain the time evolution of the diameter and charge of individual electrosprayed droplets following their initial detection. The automated data acquisition system collected large numbers of these sequences: 859 for water, 469 for acetonitrile, and 2370 for methanol. Three representative time sequences are shown in Figures 7−9 for electrosprays of water, acetonitrile, and methanol, respectively. Included in Figures 7−9 are calculated diameters for the evaporation of neutral droplets. In this size range, the change in droplet diameter, D_p, with time, t, for a pure droplet consisting on species A is proportional to droplet surface area, and is given by eq 3:[15]

$$D_p^2 = D_{p,0}^2 - 8t\frac{c_A D_{AB}}{c_p}\ln\left[\frac{1 - x_{A\infty}}{1 - x_{As}}\right] \qquad (3)$$

Here, $D_{p,0}$ is the droplet diameter at time $t = 0$, c_A is the molar concentration of species A in the vapor phase, c_p is the molar concentration of species A in the liquid phase, D_{AB} is the binary diffusivity of vapor A in gas B, and x_{As} and $x_{A\infty}$ are the mole fractions of species A at the droplet surface and far from the

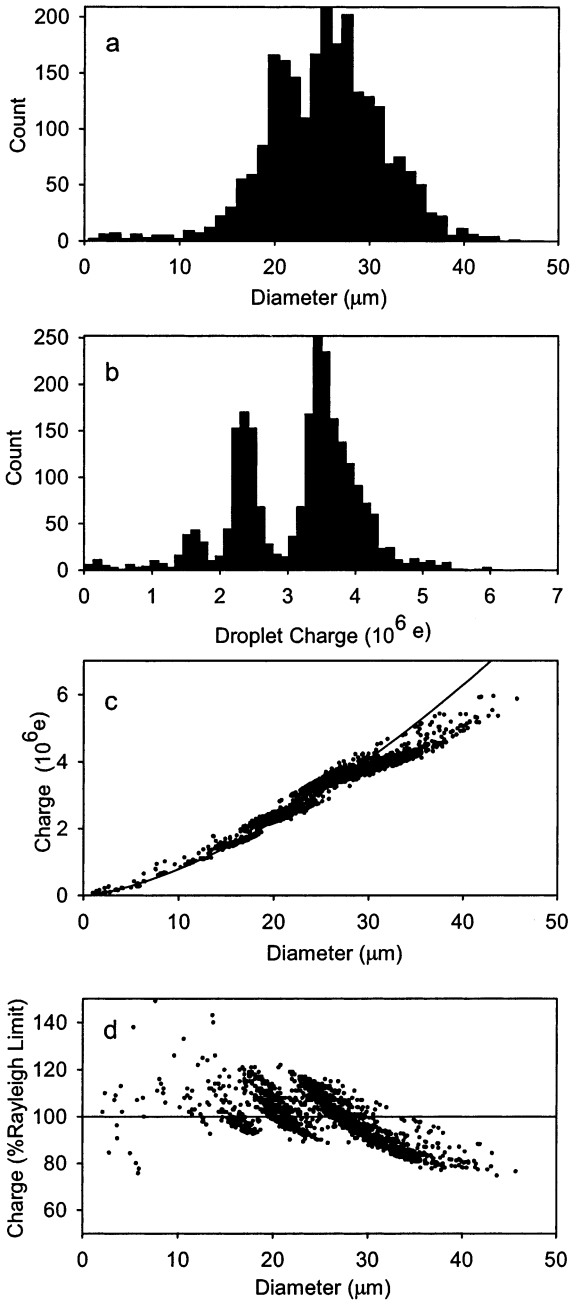

Figure 6. Plots of size and charge measurements of individual droplets in a positive-ion electrospray of pure methanol. (a) Droplet diameter histogram; (b) droplet charge histogram; (c) diameter versus charge, plotted with a curve representing the Rayleigh stability limit; (d) diameter versus charge, with charge represented as the percentage of the Rayleigh limit.

droplet, respectively. The Fuchs, Kelvin, and wind effects[15] are negligible in this size range and were therefore excluded. We used a steady-state temperature depression model[15] to calculate evaporative cooling of the droplet surface. For acetonitrile and methanol droplets evaporating in a vapor-free gas at 293 K, this depression is 25 and 28 °C, respectively. For water droplets evaporating in a vapor-free gas at 317 K, the depression is 28 °C.

Figure 7a shows the change in droplet diameter as a function of time for a water droplet. Superimposed on the experimental results are the model results for neutral water droplets at 317 K. Excellent agreement can be seen in the figure, providing strong evidence that evaporation plays a primary role in determining droplet mass loss. In Figure 7b, one can see that

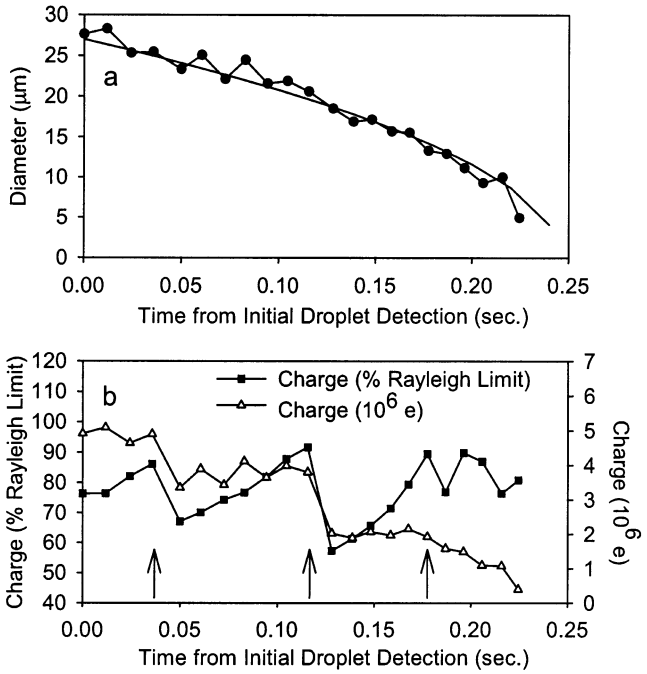

Figure 7. Evaporation and discharge of a positively charged water droplet in a 317 K N_2 buffer gas and a 51 V/cm electric field. (a) Variation of droplet diameter with time. Also plotted is the predicted evaporation dynamics of a water droplet in a vapor-free N_2 gas at 317 K. (b) Variation of droplet charge with time, represented as the number of elementary charges and as the percent of the Rayleigh limit of charge for measured droplet. Arrows indicate discharge events.

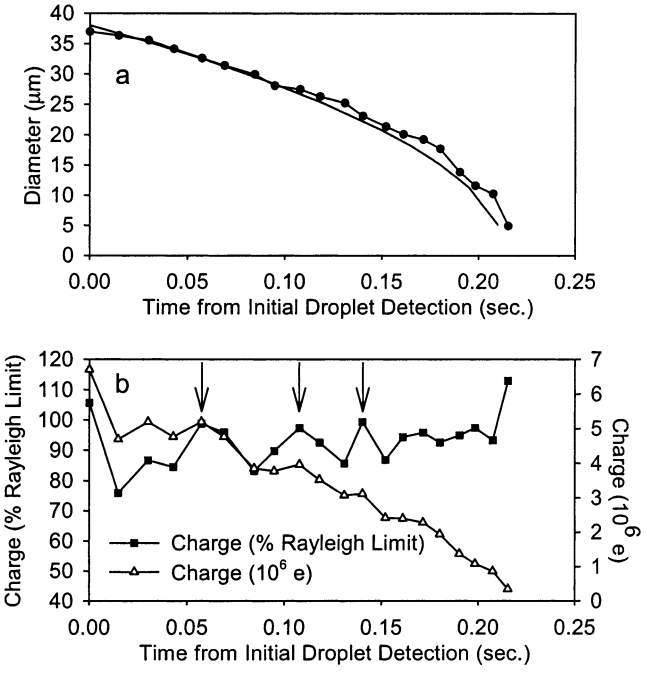

Figure 8. Evaporation and discharge of a positively charged acetonitrile droplet in a 51 V/cm electric field. Also plotted is the predicted evaporation dynamics of an acetonitrile droplet in a vapor-free N_2 gas. (a) Variation of droplet diameter with time; (b) variation of droplet charge with time, represented as the number of elementary charges and as the percent of the Rayleigh limit of charge for measured droplet. Arrows indicate discharge events.

the droplet has undergone a series of three or more discharge events (indicated by the arrows) during the course of the measurement. The discharge events depicted in Figure 7b correspond to a charge loss of 20−40% of the total charge and

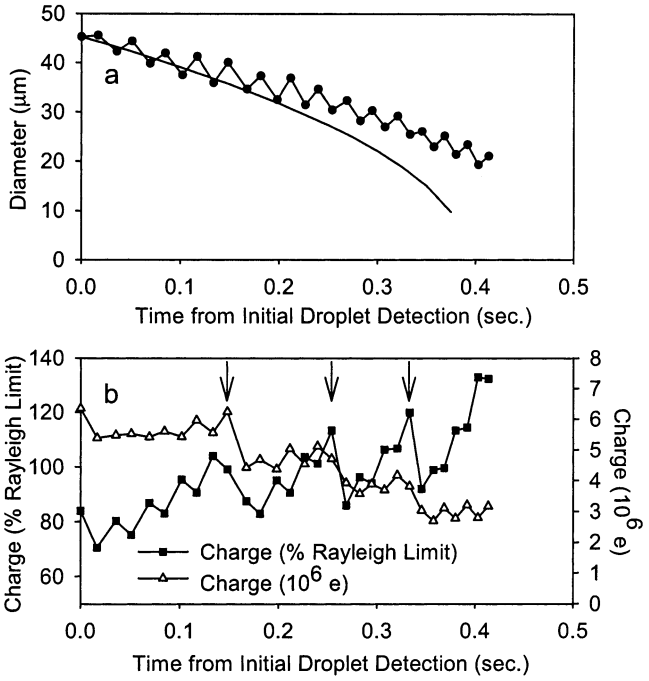

Figure 9. Evaporation and discharge of a positively charged methanol droplet (10^{-6} M NaCl added) in a 51 V/cm electric field. Also plotted is the predicted evaporation dynamics of a neutral methanol droplet in a vapor-free N_2 gas. (a) Variation of droplet diameter with time; (b) variation of droplet charge with time, represented as the number of elementary charges and as the percent of the Rayleigh limit of charge for measured droplet. Arrows indicate discharge events.

exhibit some variation between successive events. In this and other ping-pong sequences acquired for this water electrospray, no discharge events were observed at sizes greater than 20 μm during the measurement window, which starts approximately 200 ms after nascent droplet formation at the electrospray needle and continues for 250 ms until the droplet is no longer detected. This supports the interpretation given above for the size−charge correlation of Figure 4c that the droplets larger than 20 μm have not yet reached the Rayleigh limit and undergo evaporation only.

Similar droplet ping-pong sequences for acetonitrile and methanol are provided in Figures 8 and 9, respectively. The predicted droplet diameters due to evaporation alone are included in Figures 8a and 9a. The theoretical curves for evaporation dynamics slightly over-predict droplet mass loss for the case of pure methanol and, to a lesser degree, acetonitrile. This discrepancy is due to the simplicity of our surface-area controlled evaporation model and the assumptions of a vapor-free gas surrounding the droplet and constant bulk droplet temperature. The differences are nonetheless minor for all solvents studied and support the assertion that evaporative processes dominate the decrease in droplet mass with time. In no case could we discern a discrete decrease in mass at the time of a discharge event.

As previously mentioned, the discrete groupings in the size−charge correlation for methanol (Figure 6d) suggest a consistent loss of charge in each discharge event that preserves the initial tightly clustered size-charge distribution. The reproducible behavior of identical methanol droplets is demonstrated in Figure 10, where two individual charged droplets from a positive ion electrospray of methanol are displayed. These droplets were chosen for being nearly identical in the first measurement of size and charge in the ping-pong sequence. As Figure 10 demonstrates, the evaporation and discharge dynamics of the two droplets are nearly identical.

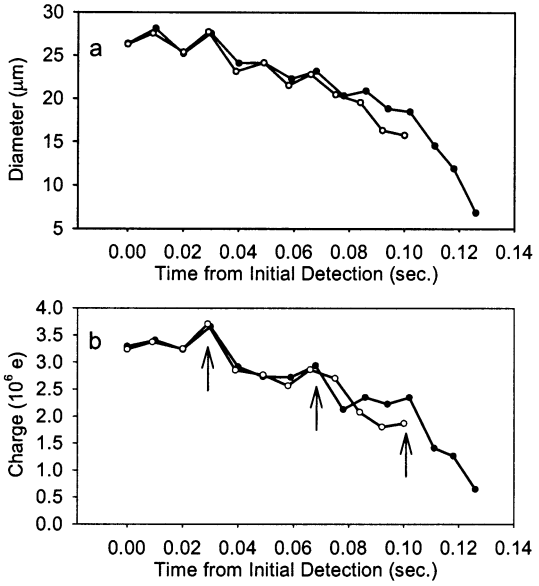

Figure 10. Evaporation and discharge of two positively charged methanol droplets with identical initial size and charge. Arrows indicate discharge events.

Droplet Charge Polarity Effects. We have studied negative-ion electrosprays of methanol to determine the influence of droplet charge polarity on the dynamics of droplet evaporation and discharge. Figure 11 presents size and charge histograms as well as size−charge correlations for a negative-ion electrospray of a solution of 10^{-4} M NaCl in methanol. The higher salt concentration was required for establishing stable negative droplet spraying conditions for these tests. The size distribution (Figure 11a) is skewed toward the smaller sizes due to evaporation. The charge distribution (Figure 11b) features a broad shoulder at smaller charge levels. The size-charge correlation in Figure 11c suggests that Rayleigh instability causes this shoulder, as droplets with charge less than 3×10^6 electrons correlate well with the curve representing the Rayleigh limit of charge. Figure 11d shows the droplet size-charge correlation, with charge represented as the percentage of the Rayleigh limit. A comparison of Figures 6d and 11d leads to the following observations. No groupings exist in the size−charge correlation of the negative-ion electrospray, unlike the case for positive-ion mode, suggesting that the disruption process with negative methanol droplets is not as repeatable or that nascent droplet formation is not monodisperse with the conditions of the experiment. Negatively charged methanol droplets reach a maximum charge level corresponding to 125−130% of the Rayleigh limit of charge, slightly higher than that attained by positively charge droplets (120%).

To investigate the dynamics of droplet evaporation and discharge in negative-ion electrospray, we conducted time evolution measurements using the ping-pong technique. For each data point in Figure 11, a time sequence was acquired resulting in 2550 individual sequences. Figure 12 shows one time sequence of size and charge. Plotted alongside the droplet diameter curve (Figure 12a) is the modeled evaporation curve for a neutral methanol droplet. The observed and modeled droplet diameters are in close agreement, indicating again that solvent loss is dominated by evaporation. Figure 12b depicts the time evolution of droplet charge. The degree of scatter in the data is generally higher than in Figures 7−9, although the source of the scatter in the droplet charge data (Figure 12b) can be traced to the scatter in the droplet diameter (Figure 12a) as given by eq 2. Generally, the observations made for positive

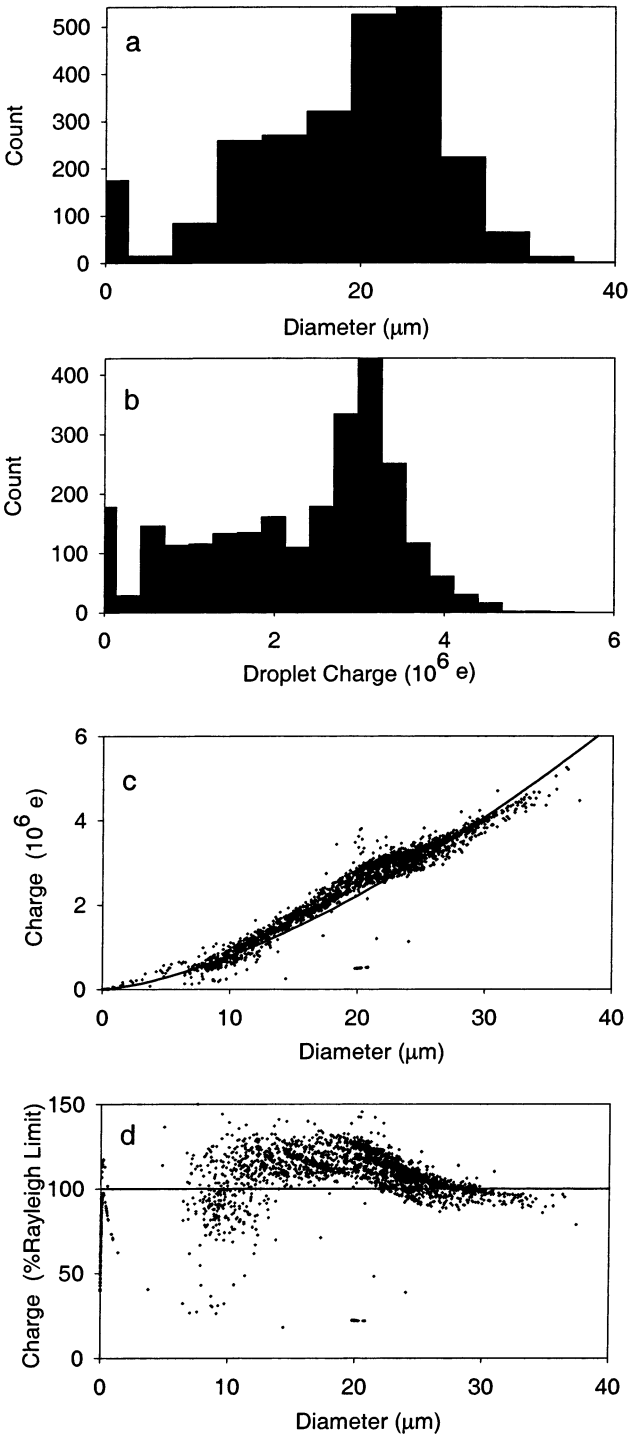

Figure 11. Diameter versus charge for a negative-ion electrospray of 10^{-4} M NaCl in methanol. (a) Droplet diameter histogram; (b) droplet charge histogram; (c) diameter versus charge, plotted with a curve representing the Rayleigh stability limit; (d) diameter versus charge, with charge represented as the percentage of the Rayleigh limit.

droplets from the previous section apply in the case of negative droplets. Each discharge event is characterized by a loss of 20−30% of droplet charge and no detectable change in droplet diameter.

Electrolyte Concentration Effects. Electrolyte concentrations in electrospray ionization typically span a wide range. We report here an investigation of droplet discharge processes in positive-ion electrosprays of salt−methanol solutions. The objective of this part of the investigation is to determine if electrolyte levels influence the mechanism or dynamics of

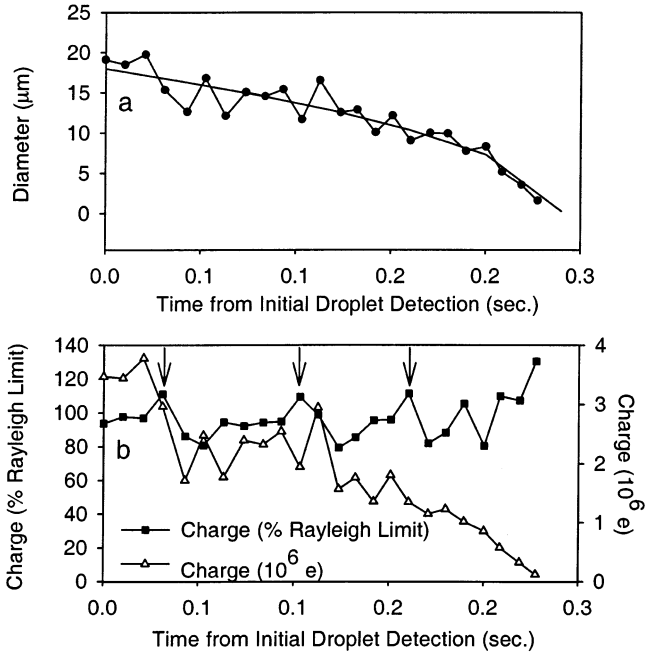

Figure 12. Evaporation and discharge of a negatively charged droplet of methanol in a 51 V/cm electric field. Also plotted is the predicted evaporation dynamics of a neutral methanol droplet in a vapor-free N_2 gas. (a) Variation of droplet diameter with time; (b) variation of droplet charge with time, represented as the number of elementary charges and as the percent of the Rayleigh limit of charge for measured droplet. Arrows indicate discharge events.

droplet discharge. NaCl was added to spectroscopic grade methanol to create solutions with concentrations of 10^{-6}, 10^{-5}, and 10^{-4} M. Although we did not measure the electrical conductivity of solutions prior to each test, extra care was taken to minimize sample contamination through the use of fresh solutions, clean glassware, and minimized handling. During these investigations, we found that the weaker salt solutions were more stable and easier to characterize. Figure 13 shows the size-charge correlations for these electrosprays. In Figure 13a, corresponding to 10^{-6} M NaCl, one can observe the same groupings that were seen above in Figure 6d. This structure is not seen for the higher salt concentrations (Figure 13, parts b and c).

Despite the differences in the size and charge distributions for different electrolyte concentrations, the results of ping-pong measurements show little difference in evaporation and discharge dynamics for varying salt concentrations. Figure 14 demonstrates this point. To create the plots shown in the figure, we have searched our database of ping-pong measurements made for all three electrolyte concentrations to find the best match in the first size and charge measurement. The results presented in Figure 14 show evaporation and discharge sequences at each concentration level for droplets with initial measured diameter lying within 26 ± 0.5 μm and charge within $(3.2 \pm 0.5) \times 10^6$ electrons. Figure 14a shows the superposition of droplet diameter versus time and does not reveal a correlation between electrolyte level and evaporation rate. The plot of the time evolution of droplet charge (Figure 14b) shows some variability in the times at which the droplets undergo discharge. However, the charge level at which disruption occurs is approximately equal for all three electrolyte levels (115−120% of the Rayleigh limit of charge). We attribute the difference in the time at which disruption occurs to the criteria we establish for locating these "matched" sequences. Better statistics would allow for a better initial size and charge match for all three

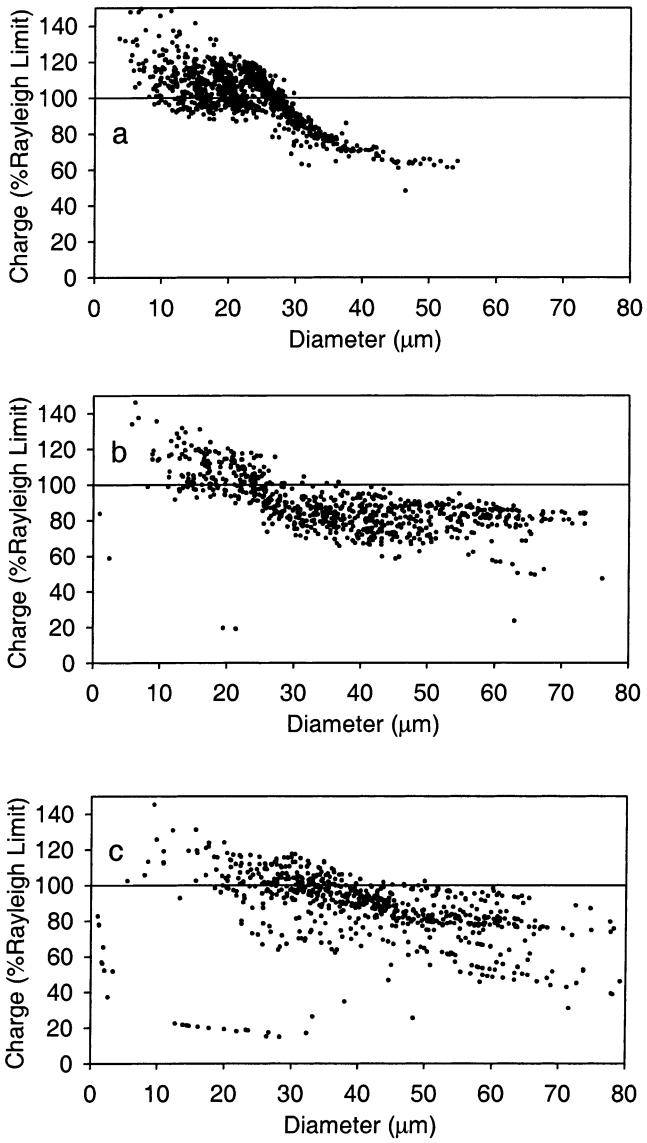

Figure 13. Diameter versus charge, with charge represented as the percentage of the Rayleigh limit, for a positive-ion electrospray of methanol with the following concentrations of NaCl: (a) 10^{-6}, (b) 10^{-5}, and (c) 10^{-4} M.

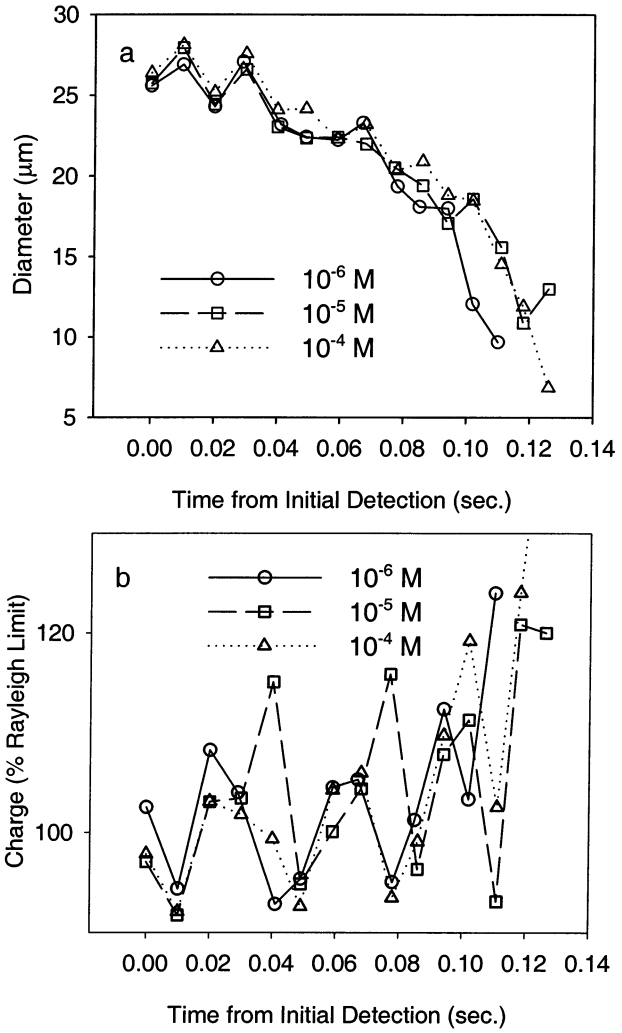

Figure 14. Evaporation and discharge of positively charged droplets of 10^{-6}–10^{-4} M NaCl in methanol in a 51 V/cm electric field. (a) Variation of droplet diameter with time; (b) variation of droplet charge with time, represented as the percent of the Rayleigh limit of charge for measured droplet size.

charge levels. Nevertheless, the data in Figure 14b do not indicate any marked effect of electrolyte concentration over the range 10^{-6}–10^{-4} M on droplet discharge dynamics.

Discussion

The ability of the PDI to obtain the instantaneous size and charge measurements shown in Figures 4–6 provides unique insights into the process of electrospray ionization. Droplets are formed at the source with a distribution of size and charge defined by the spray conditions. Here, cone jet mode conditions suggest that the distributions are pseudomonodisperse, although we did not confirm this with additional measurements. The broad size histogram in the case of water (Figure 4) resembles that of Chen et al. for "pulsating mode" conditions,[34] suggesting that the water electrospray may have been operating in pulsating mode. Droplet discharge is evident in all of the size–charge correlations. Except for water, this happens generally above the Rayleigh limit, as evident in Figures 5c and 6c–d where the data exceed the Rayleigh limit in charge by 10–20%. The observation that discharge occurs at or above the Rayleigh limit of charge contrasts the observations made with the EDB, which almost unanimously report discharge events at 60-90% of the Rayleigh limit of charge (see Table 1). However, as Gomez and Tang point out,[23] the surface tension of a droplet near the Rayleigh limit approaches zero so that even a small external disturbance might initiate droplet disruption. The techniques employed in this study represent gentle environmental conditions for the droplets, with Weber numbers (defined as the ratio of inertial to surface tension forces) for the solutions studied here on the order of 10^{-5}, 5 orders of magnitude lower than that which might lead to droplet distortion. Also, in the ping-pong experiment, the laser beam used to probe droplet properties is in contact with the droplet momentarily every 10–20 ms, so radiant heating of the droplet should be much less than that which may occur with EDB studies where the beam is in contact with the droplet continuously.

The higher volatility of acetonitrile and methanol, resulting in size–charge correlations that include droplets that have undergone one or more discharge event, allows for the direct measurement of charge loss associated with the Rayleigh instability. This is seen in Figures 5c and 6c, where the range of charge for a given droplet diameter can be directly measured. This charge loss can also be observed in Figures 6d and 13a as the vertical spaces that separate the three groups of data. The

charge loss amounts to approximately 20% of the total droplet charge prior to breakup. This is consistent with most studies of droplet discharge for less volatile solutions (see Table 1) but contrasts distinctly with the recent study by Feng et al.,[20] who report charge loss for a methanol/10^{-5} M NaCl solution of 81%. It is interesting to note the difference between the size-charge correlation of methanol and those of water and acetonitrile. Because the cone jet spray conditions that lead to the formation of nascent droplets are the same for all three, one would expect to see similar size-charge correlations that differ only by the onset of Rayleigh instability. The observation that water and acetonitrile have size-charge correlations that span a continuous range of size and charge, whereas methanol forms discrete groups, suggests that, for methanol, (1) it is easier to achieve spray conditions with monodisperse droplet size and (2) the evaporation and discharge dynamics for methanol are more consistently reproducible than for water and acetonitrile.

The time evolution of droplet diameter and charge provided by the ping-pong experiment as shown in Figures 7−9 provides a more complete picture of droplet evaporation and discharge dynamics. Droplet size decreases according to evaporation models developed for neutral liquid aerosol droplets. During evaporation, the overall charge on the droplet is conserved, also consistent with the observations of other investigators.[16,17,44] The Rayleigh limit (eq 1) is quite accurate in predicting the onset of droplet instability for the case of water and underestimates the onset of disruption for the case of acetonitrile and methanol. Discharge events occur by loss of 15−20% of the droplet charge in the case of methanol and acetonitrile and 20−40% in the case of water. For all solutions, the time sequences show no detectable discrete change in droplet diameter correlated with observed discharge events. Consideration of the mass loss associated with discharge reported by other investigators in Table 1 indicates that less than 0.7% uncertainty in the diameter measurement of the PDI would be required to detect the 2% mass change reported by most investigators. Because the instrument used for the present studies has an uncertainty of about 5%, it is not surprising that we are not able to detect a size change as a result of disruption.

We can estimate the number of progeny droplets created as a result of disruption by analyzing the measured charge loss associated with each discharge, and by adopting the value proposed by Loscertales and Fernandez de la Mora[27] for the charge of the newly formed progeny droplets of 0.7 times the Rayleigh limit of charge for the newly formed droplet. We take the approach here of Tang and Smith[45] and calculate the progeny droplet size as a function of the number of identically sized progeny droplets. We use the data in Figure 6d to calculate the average diameter and charge loss corresponding to the first, second, and third discharges. The result is plotted in Figure 15. If we assume that the progeny droplets are of a diameter that is 10% of the parent droplet,[23] then approximately four progeny droplets are created as a result of methanol disruption. This value falls in the middle of the range reported by a modeling study of the process,[46] which reported a range from two to seven. It is less than the average number of 13 observed recently by Feng et al.[20] in their EDB study of methanol. For larger droplets undergoing discharge, the PDI might have been able to detect the progeny droplets. However, no evidence was seen for their presence in the observation volume.

As mentioned previously, earlier theoretical and experimental studies have reported that the electrical conductivity of the solution influences the total ion current from the spray plume[32] and the ion current emitted from individual discharge events.[35]

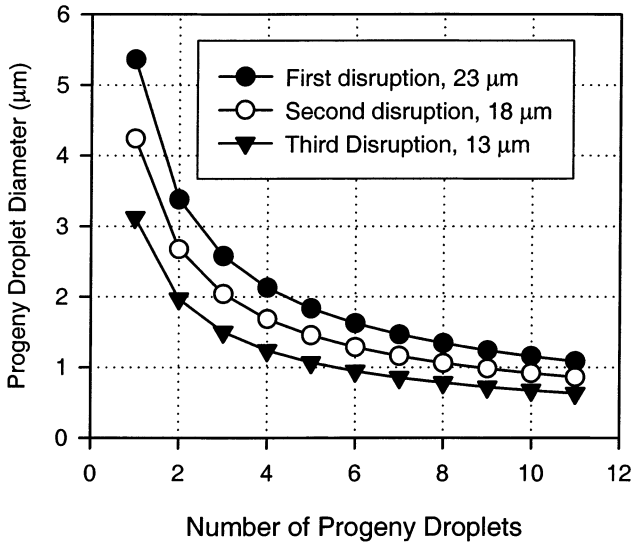

Figure 15. Diameter of progeny droplets as a function of the number produced, based on data in Figure 6d (see text). Droplet diameters in legend correspond to the average diameters at which disruptions occur.

In view of this result, it would seem that a variation in the electrolyte concentration from 10^{-6}−10^{-4} M investigated in the current study would make a noticeable difference in the observed mechanism of droplet discharge. This has not been demonstrated by our observations, from which we conclude that the range of electrolyte concentrations used in typical electrosprays affects the mechanism and dynamics of the discharge process very little.

One notable result of observations of droplet disruption using the ping-pong technique is that it is possible to monitor a highly charged droplet through several fission events despite having no radial trapping field. If the ejection of mass during fissioning has no preferred direction, then the observation that the parent droplet does not acquire significant translational energy can be used to quantify the impulse imparted to a droplet as a result of Rayleigh instability. If, however, the direction of disruption were primarily axial, then even a highly energetic process would result in minimal radial displacement and would be consistent with our observations. Further study is needed to determine the direction of disruption for a droplet trapped in the ping-pong apparatus, perhaps by the addition of an imaging apparatus for taking photomicrographs of the fission process.

Conclusion

We have presented an experimental technique for measuring the droplet size and charge of individual electrosprayed droplets using phase Doppler measurements of these droplets as they reside in a uniform electric field. Using the ping-pong technique, one can obtain time series of droplet size and charge. These time series plots complement the observed distribution of size and charge from the electrospray source measured at a single spatial location. The results are summarized as follows: (1) The discharge dynamics of droplets with the same initial diameter and charge are highly reproducible for methanol and show somewhat more stochastic behavior for electrosprays of water and acetonitrile. (2) Published over a hundred years ago, Rayleigh's analysis of charged droplet instabilities resulting from solvent evaporation is remarkably accurate in predicting observed discharge events for all three solvents. Discharge for electrosprays of water occur very near the Rayleigh limit, and those for methanol and acetonitrile occur at 100−120% of the Rayleigh limit. (3) Droplet discharge events are characterized by loss of 15−20% of the charge from methanol and acetonitrile droplets and 20−40% from water droplets, with little ac-

companying loss of solvent. (4) The addition of salt (up to 10^{-4} M) to the solution does not significantly affect the discharge dynamics. The size−charge correlation and discharge dynamics of negatively charged droplets formed in electrospray ionization of 10^{-4} M NaCl in methanol are similar to those observed for positively charged droplets. (5) The life history of a single electrosprayed droplet can be followed through numerous discharge events (sequences with up to 50 measurements and 6 discharges have been observed) in the absence of radial confinement. If the direction of droplet disruption is random, then this implies that no significant displacement of the droplet arises from discharge events and is inconsistent with any notion of high-energy chaotic fission processes. (6) The discrete transitions in the methanol droplet size-charge correlation suggest nearly monodisperse nascent drop formation. The consistent loss of charge in each discharge event preserves the initial tightly clustered size-charge distribution.

Although the present investigation focuses on the processes of evaporation and discharge in electrosprayed droplets using common solvents, the droplet ping-pong technique can probe the evaporation and discharge dynamics of droplets irrespective of their volatility. These experimental methods lay the groundwork for further investigations covering a variety of issues. We can investigate the effects of binary liquid mixtures on the electrospray mechanism, applying this to the observations of Iavarone et al., that the addition of glycerol or *m*-nitrobenzyl alcohol into the electrospray solutions creates "supercharged" proteins with dramatically increased charge state and abundance.[47] We can also investigate the affect that surface-active agents may have in the discharge dynamics of electrospray solutions. Davis and Bridges have suggested that there is a discrete transition in evaporation dynamics when a monolayer of surfactant is formed on the droplet surface,[48] suggesting a means for tuning the electric field at the droplet surface to favor the detection of analyte compounds with differing surface activities. The mobility cell used in these investigations is already configured for investigations into the distribution of progeny droplets using elastic light scattering or laser-induced fluorescence (LIF) techniques, the latter of which has already been applied to the study of electrospray plume cross-sections.[49] Similar LIF techniques have been used to investigate chemical changes in the electrosprayed droplets at various locations in the plume[50] and gas-phase ion formation from liquid sample droplets in an inductively coupled plasma,[51] and the ping-pong technique would appear to be ideally suited for these types of LIF measurements. We also envision the attachment of an orthogonal sampling time-of-flight mass spectrometer to the end of the drift cell to analyze ions from individual discharge events of single droplets. Similar approaches have been taken by investigators using an EDB for sample preparation[52] and using free-falling monodispersed droplets passing by a corona discharge needle.[53]

Acknowledgment. The authors thank the following agencies for funding this work: National Science Foundation (CHE-9727566), Defense Advanced Research Projects Agency, the Office of Naval Research, and the Beckman Institute of Caltech.

References and Notes

(1) *Electrospray Ionization Mass Spectrometry: Fundamentals, Instrumentation, and Applications*; Cole, R. B., Ed.; John Wiley and Sons: New York, 1997.
(2) Rayleigh, L. *Proc. R. Soc.* **1882**, *14*, 184−86.
(3) Mann, M. *Org. Mass Spectrom.* **1990**, *25*, 575−587.
(4) Kebarle, P. *J. Mass Spectrom.* **2000**, *35*, 804−817.
(5) Constantopoulos, T. L.; Jackson, G. S.; Enke, C. G. *Anal. Chim. Acta* **2000**, *406*, 37−52.
(6) de la Mora, J. F. *Anal. Chim. Acta* **2000**, *406*, 93−104.
(7) Fenn, J. B.; Rutan, S. C. *Anal. Chim. Acta* **2000**, *406*, 1−1.
(8) Gamero-Castano, M.; de la Mora, J. F. *Anal. Chim. Acta* **2000**, *406*, 67−91.
(9) Kaufman, S. L. *Anal. Chim. Acta* **2000**, *406*, 3−10.
(10) Kebarle, P.; Peschke, M. *Anal. Chim. Acta* **2000**, *406*, 11−35.
(11) Gamero-Castano, M.; de la Mora, J. F. *J. Mass Spectrom.* **2000**, *35*, 790−803.
(12) de la Mora, J. F.; Van Berkel, G. J.; Enke, C. G.; Cole, R. B.; Martinez-Sanchez, M.; Fenn, J. B. *J. Mass Spectrom.* **2000**, *35*, 939−952.
(13) Kebarle, P. *J. Mass Spectrom.* **2000**, *35*, 804−817.
(14) Taylor, G. *Proc. R. Soc. A* **1964**, *280*, 383−397.
(15) Davis, E. J. Microchemical engineering: the physics and chemistry of the microparticle. In *Advances in Chemical Engineering*; Drew, T. B., Ed.; Academic Press: New York, 1992; Vol. 18.
(16) Abbas, M. A.; Latham, J. *J. Fluid Mech.* **1967**, *30*, 663−670.
(17) Taflin, D. C.; Ward, T. L.; Davis, E. J. *Langmuir* **1989**, *5*, 376−384.
(18) Davis, E. J.; Bridges, M. A. *J. Aerosol Sci.* **1994**, *25*, 1179−1199.
(19) Richardson, C. B.; Spann, J. F. *J. Aerosol Sci.* **1984**, *15*, 563−571.
(20) Feng, X.; Bogan, M. J.; Agnes, G. R. *Anal. Chem.* **2001**, *73*, 4499−4507.
(21) Bauckhage, K. *Part. Part. Syst. Charact.* **1988**, *5*, 16−22.
(22) Bachalo, W. D.; Houser, M. J. *Opt. Eng.* **1984**, *23*, 583.
(23) Gomez, A.; Tang, K. Q. *Phys. Fluids* **1994**, *6*, 404−414.
(24) Olumee, Z.; Callahan, J. H.; Vertes, A. *J. Phys. Chem. A* **1998**, *102*, 9154−9160.
(25) Naqwi, A. A.; Hartman, R. P. A.; Marijnissen, J. C. M. *Part. Part. Syst. Charact.* **1996**, *13*, 143−149.
(26) Macky, W. A. *Proc. R. Soc. A* **1931**, *133*, 565−586.
(27) Loscertales, I. G.; Fernandez de la Mora, J. *J. Chem. Phys.* **1995**, *103*, 5041−60.
(28) Gamero-Castano, M.; de la Mora, J. F. *J. Chem. Phys.* **2000**, *113*, 815−832.
(29) Hinds, W. C. *Aerosol technology: properties, behavior, and measurement of airborne particles*, 2nd ed.; John Wiley and Sons: New York, 1999.
(30) Hirabayashi, A.; de la Mora, J. F. *Int. J. Mass Spectrom.* **1998**, *175*, 277−282.
(31) Thomson, B. A.; Iribarne, J. V. *J. Chem. Phys.* **1979**, *71*, 4451−4463.
(32) Tang, L.; Kebarle, P. *Anal. Chem.* **1991**, *63*, 2709−2715.
(33) Gañán-Calvo, A.; Dávila, J.; Barrero, A. *J. Aerosol Sci.* **1997**, *28*, 249−275.
(34) Chen, D.-R.; Pui, D. Y. H.; Kaufman, S. L. *J. Aerosol Sci.* **1995**, *26*, 963−977.
(35) delaMora, J. F. *J. Colloid Interface Sci.* **1996**, *178*, 209−218.
(36) Grace, J. M.; Marijnissen, J. C. M. *J. Aerosol Sci.* **1994**, *25*, 1005−1019.
(37) SIMION; Ion Source Software: Ringoes, NJ, 1998.
(38) Smith, J. N. *A: Computational Chemistry Applied to the Analysis of Air Pollution Reaction Mechanisms; B: Fundamental Studies of Droplet Evaporation and Discharge Dynamics in Electrospray Ionization.* Ph.D., California Institute of Technology, Pasadena, CA, 2000.
(39) Wriedt, T.; Jiang, Z.; Rheims, J.; Warncke, N.; Duersterbeck, F. SCATAP for Windows; Stiftung Institut fuer Werkstofftechnik: Bremen, Germany, 1996.
(40) Chigier, N. *Combustion Measurements*; Hemisphere Pub. Corp.: Washington, DC, 1991; Vol. XIV.
(41) *LabVIEW*; National Instruments Corp.: Austin, TX, 1998.
(42) Rajaona, R. D.; Sulmont, P. *J. Comput. Phys.* **1985**, *61*, 186−193.
(43) Flagan, R. C.; Seinfeld, J. H. *Fundamentals of Air Pollution Engineering*; Prentice Hall: New York, 1988.
(44) Law, S. E. *IEEE Trans. Ind. Appl.* **1989**, *25*, 1081−1087.
(45) Tang, K. Q.; Smith, R. D. *Int. J. Mass Spectrom.* **1999**, *187*, 97−105.
(46) Roth, D. G.; Kelly, A. J. *IEEE Trans. Ind. Appl.* **1983**, *IA-19*, 771−775.
(47) Iavarone, A. T.; Jurchen, J. C.; Williams, E. R. *Anal. Chem.* **2001**, *73*, 1455−1460.
(48) Davis, E. J.; Bridges, M. A. *J. Aerosol Sci.* **1994**, *25*, 1179−1199.
(49) Zhou, S.; Edwards, A. G.; Cook, K. D. *Anal. Chem.* **1999**, *71*, 769−776.
(50) Zhou, S. L.; Cook, K. D. *Anal. Chem.* **2000**, *72*, 963−969.
(51) Olesik, J. W.; Kinzer, J. A.; McGowan, G. J. *Appl. Spectrosc.* **1997**, *51*, 158A-175A.
(52) Bogan, M. J.; Agnes, G. R. *Anal. Chem.* **2002**, *74*, 489−496.
(53) Hager, D. B.; Dovichi, N. J.; Klassen, J.; Kebarle, P. *Anal. Chem.* **1994**, *66*, 3944−3949.
(54) Richardson, C. B.; Pigg, A. L.; Hightower, R. L. *Proc. R. Soc. A* **1989**, *422*, 319−328.
(55) Schweitzer, J. W.; Hanson, D. N. *J. Colloid Interface Sci.* **1970**, *35*, 417−423.